Journal of Materials Chemistry B

Accepted Manuscript

ROYAL SOCIETY OF CHEMISTRY

www.rsc.org/materialsB

Aptamer-functionalized graphene oxide for high efficient loading and cancer cell-specific delivery of antitumor drug

Yimei Lu,[a] Ping Wu,*[a] Yajing Yin,[a,b] Hui Zhang,[a] and Chenxin Cai*[a]

[a] Jiangsu Key Laboratory of New Power Batteries, Jiangsu Collaborative Innovation Center of Biomedical Functional Materials, College of Chemistry and Materials Science, Nanjing Normal University, Nanjing 210097, P. R. China.

[b] Jiangsu Second Normal University, Nanjing 210013, P. R. China.

* Corresponding author, E-mail: wuping@njnu.edu.cn, cxcai@njnu.edu.cn (C. Cai)

Electronic supplementary information (ESI) available: Details on cell culture, MTT and LDH assays, detailed analysis on the hydrogen bonds formed between GO and DAC at different pH, and seven figures.

ABSTRACT: This work reports a novel anticancer drug loading and cell-specific delivery system based on cell-type-specific aptamer-functionalized graphene oxide (GO) using decitabine (DAC) and A549 cell as anticancer drug and target cell model, respectively. We conjugated GO with aptamer A1 (a 45-base oligonucleotide binds to A549 cell with high specificity and affinity) and then loaded DAC onto surface of GO (A1–GO/DAC complexes). The loading capacity of DAC on GO surface is pH- and DAC initial concentration-dependent, the saturated loading capacity, as high as ~3.0 mg DAC/mg GO (corresponding to the loading efficiency of ~64%), is attained at physiological condition (pH 7.4) and DAC initial concentration of higher than 0.7 mg/mL. The release of DAC from the complexes is also pH-dependent, and DAC is released at a quicker rate at acidic pH condition (pH 5.5) than at physiological pH condition. The complexes can specifically recognize A549 cells from other types of cancer cells and subtypes of lung cancer cells due to the specific binding of the aptamer with the cells. Importantly, cell viability assay results reveal that the complex displays a much higher therapeutic efficacy in inhibiting the growth of the cancer cells by inducing the cell membrane damage than free DAC drug. The high DAC payload and antitumor efficacy render our developed system promising for different biomedical applications.

Keywords: Decitabine; Graphene oxide; Aptamer; Cancer therapy; Drug delivery.

1. Introduction

Cancer is a growing health problem around the world, particularly with the steady rise in life expectancy, increasing urbanization, and the subsequent changes in environmental conditions and lifestyle.[1] Although the mortality has decreased in the past few years with the improvement of diagnostic equipments and therapeutic technology, chemotherapy, alone or combined with radiotherapy, often kills healthy cells and thus shows significant toxicity and unavoidable side effects due to that traditional anticancer drugs cannot discern between diseased and healthy cells.[2] Moreover, the drug dose within cancerous cells is always limited due to the non-specific, non-targeted nature of most of the anticancer drugs and their inadequate delivery to tumor tissues.

To improve the therapeutic index of drugs, much effort has been made to develop drug carriers for tumor-targeted delivery. Up to date, variable forms of drug carriers have been developed, including inorganic materials (such as gold nanoparticles,[3,4] quantum dots,[5,6] carbonaceous materials,[7-12] porous silica materials,[2,13,14] selenium nanopartilces,[15] mesoporous stronitium hydroxyapatite,[16] and laponite nanodisks[17] etc.), inorganic-polymeric hybridized materials (such as graphene oxide-polyethylenimine,[18] and iron oxide-polypyrrole nanoparticles[19] etc), and lipsomes[20] etc. Although these drug carriers have shown many advantages such as drug solubilization and prolonged blood circulation, there are several obstacles during the transport process of drug delivery systems to tumor cells, such as lack of the ability to achieve high targeting efficiency at tumor sites, insufficient cell uptake, and nonspecific accumulation in normal tissues leading to serious side effects and thus limiting their clinical usage.

The therapeutic efficacy of drugs would be significantly improved if the drug carriers are conjugated with tumor-targeting ligand units that can specifically recognize molecular signatures on cancer cell surface. Such a tumor-targeting strategy, exploiting cancer specific biomarkers, would minimize systemic toxicity and, thereby, undesirable side effects typically associated with conventional chemotherapy. Targeting ligands that can serve such a purpose include peptides,[21] transferrin,[22] polysaccharides (e.g. hyaluronic acid),[23] vitamins (e.g. folic acid or biotin),[10,24,25] and monoclonal antibodies[26,27] etc. However, the use of these ligands as cell-specific homing agents poses significant

challenges. They are difficult to control and typically show poor site specificity for the conjugation and inconsistent binding affinity.[28] They also tend to be immunogenic,[29] and thus require extra humanization steps, which make them difficult for handle and application.

We report here a novel anticancer drug loading and cell-specific delivery system based on aptamer-functionalized graphene oxide (GO). Aptamers are short, single stranded DNA or RNA that could form unique 3-dimensional structures that specifically recognize a wide variety of targets from small organic molecules, proteins, cells to complex living organisms with high affinity.[30–35] However, there are scarce reports on the drug loading and release system by employing the aptamer as a specific cell targeting regent.[16] GO has attracted great attention in biomedical fields because of its biocompatible without obvious toxic effects in vivo (it has been reported that GO has no obvious cytotoxicity at a concentration of below 80 μg/mL).[36–38] In particular, its abundant hydrophilic groups, outstanding water solubility, and the larger specific surface areas have enabled GO a promising material as a drug carrier.[9–11] We employed decitabine (DAC, 5-aze-2′-deoxycytidine) and A549 cell as anticancer drug and target cell model, respectively. DAC, a nucleoside analogue that is converted intracellularly to the corresponding 5′-triphosphate and serves as a substrate for DNA replication,[39] is currently used clinically for the treatment of myelodysplastic syndromes,[40] and is in clinical trial for chronic myelogenous leukemia, lungs, esophagus, pleura, and sickle cell anemia.[41,42] A549 cell is the lung adenocarcinoma cell, which is the most prevalent non-small cell lung cancer (NSCLC, comprising ~80% of lung cancers).[43,44] We conjugated GO with the aptamer A1 (a 45-base oligonucleotide binds to A549 cell with high specificity and affinity with dissociation constants in the nanomolar range[45]) and then loaded DAC onto surface of GO. The loading and release features of the drug on GO surface are studied in details. The DAC-loaded A1–GO complexes (A1–GO/DAC) can specifically recognize A549 cells from other types of cancer cells and subtypes of lung cancer cells, bind with the cells and release the drug, and finally cause the cell death by inducing the cell membrane damage. Cell viability assay reveals the therapeutic efficacy of the complex is much higher than free DAC drug.

The advantage of this work is to use the aptamer as a cell targeting agents. Compared to other targeting agents (for example antibodies), aptamer has several attractive features such as ease of synthesis and scaling up, stability in harsh biological environments, lack of immunogenicity, rapid tissue penetration, and high affinity to targets. Moreover, they can be gradually degraded by nucleases and cleared from the blood to cause minimal system toxicity. Functionalization of aptamers to facilitate site-specific conjugation is also straightforward.[30,31] These advantages make our developed targeted drug-delivery systems a great potential for different biomedical applications.

2. Experimental section

2.1. Chemicals

Decitabine (DAC), *N*-(3-dimethylaminopropyl)-*N*′-ethylcarbodiimide (EDC), *N*-hydroxysuccinimide (NHS, 98%), and (3-(4,5-dimethyl-2-thiazolyl)-2,5-diphenyl-2H-tetrazolium bromide) (MTT, >98%) were from Sigma-Aldrich and used as received. Oligonucleotides were purchased from *BioSune* Biological Engineering Technology Co. (Shanghai). Their sequences were summarized in Table 1.

Table 1. The sequences of oligonucleotide used in this work

description	Sequence
aptamer (A1): 45-base single-stranded DNA. It binds to A549 cell with high specificity and affinity with dissociation constants in the nanomolar range.[45]	5′-GGT TGC ATG CCG TGG GGA GGG GGG TGG GTT TTA TAG CGT ACT CAG-$(CH_2)_6$-NH_2-3′
one-base mismatched DNA (A2): 45-base single-stranded DNA. It has one mismatched base in comparison with A1. The mismatched base was underlined.	5′-GGT TGC ATG CCG TGG GGA GGG GGG AGG GTT TTA TAG CGT ACT CAG-$(CH_2)_6$-NH_2-3′
three-base mismatched DNA (A3): 45-base single-stranded DNA. It has three mismatched bases in comparison with A1.	5′-GGT TGC ATG ACG TGG GGA GGG GGG AGG GTT TTA TAG AGT ACT CAG-$(CH_2)_6$-NH_2-3′
sgc8 aptamer: 44-base single-stranded DNA. It is specific for CEM cells.[32]	5′-ATC TAA CTG CTG CGC CGC CGG GAA AAT ACT GTA CGG TTA GA-$(CH_2)_6$-NH_2-3′
tdo5 aptamer: 47-base single-stranded DNA. It is specific for acute lymphoblastic leukemia B-cells.[46]	5′-AAC ACC GGG AGG ATA GTT CGG TGG CTG TTC AGG GTC TCC TCC CGG TG-$(CH_2)_6$-NH_2-3′

2.2. Preparation of GO and aptamer conjugation

GO was prepared from graphite powder (99.998%, 325 mesh, Alfa Aesar) using the previous reported procedures.[47,48] The prepared GO sheet is rippled and resemble crumpled silk veil waves (TEM image,

Fig. S1a, ESI) with a thickness of ~0.8 nm (AFM image, Fig. S1b, ESI), and has a C/O ratio of ~1.8, which was estimated by integrating the C1s peak and O1s peak in XPS (Fig. S1c, ESI). The C1s peak contains C–C (~284.6 eV), C–O (~286.8 eV), C=O (~287.6 eV), and O–C=O (~288.9 eV)[49] elements as evidenced from the deconvolution analysis (Fig. S1d, ESI), suggesting the single layer nature of the synthesized GO. Before conjugation of A1, GO was cut into small pieces with a size of ~20 nm (Fig. S2, ESI) by following steps: GO solution was sonicated for 1 h (400 W) and hydrothermally treated, then centrifuged (14000 rpm) for 30 min. This process was repeated for three times.

A1 was covalently conjugated to GO via the formation of the amide between –COOH group of GO and $-NH_2$ moiety at A1 by EDC/NHS chemistry. We first activated GO in EDC-NHS mixture (5 mM EDC, 10 mM NHS in PBS, pH 7.4) by dispersing 0.5 mg GO in 1 mL PBS and stirred for 30 min. After that, 10 μL of A1 (1 μM) was added to GO solution and stirred for 3 h at ambient temperature. A1–GO was collected by centrifugation and dried in vacuum solution at ambient temperature for further characterization and use.

2.3. Drug loading and release behaviors of A1–GO

Loading of DAC onto the A1–GO was carried out by stirring the mixture of DAC solution (0.05 mg/mL, in PBS, pH 7.4) and A1–GO dispersed solution (0.15 mg/mL) for 12 h. The A1–GO/DAC complexes were collected by centrifugation and rinsed with water for three times to remove those unloaded DAC, air-dried, and stored in dark before use. To evaluate the loading capacity of DAC, we collected the supernatants at each time centrifugation, and analyzed the free DAC concentration in the supernatants based on UV–vis absorbance at the wavelength of 240 nm using the molar extinction coefficient of 6900 M^{-1} cm^{-1}.[39] We calculated the loading capacity according to: drug loading capacity = mass of loaded drug / mass of A1–GO. The drug capacity was optimized by changing DAC concentrations (0.05–0.8 mg/mL) while the A1–GO concentration was kept at 0.15 mg/mL.

The release kinetics of DAC from A1–GO/DAC complexes was evaluated in PBS under pH 5.5, 7.4, and 9.0, and in cell culture medium (10% FBS/DMEM) at 37 °C. A1–GO/DAC (0.5 mg) was dispersed into 1 mL of PBS, after 10 s vortexing, the mixture was immediately placed in a dialysis bag with a

molecular weight cutoff of 3500 Da, and dialyzed against the corresponding buffer solution (10 mL) in a sample vial. The solution was kept under constant stirring. At each predetermined time interval, 1 mL of PBS solution was taken out from vial, and equal volumes of respective fresh buffer solution were replenished. The released DAC was quantified based on UV−vis absorbance at 240 nm. The percentage of drug released was evaluated by: percentage of drug released = mass of drug released / mass of drug loaded × 100%.

2.4. Anticancer activity assay

For the cell-imaging test, A549 cells (the details on cell culture are depicted in ESI) with a density of ~1 × 10^4 cells/well were seeded into a 12-well assay plate and cultured overnight to bring the cells to confluence. Then the culture medium was replaced with fresh medium containing 20 μg/mL A1–GO/DAC and incubated at 37 °C for 2 h. After the cells were washed with PBS to remove unbound complexes, the images were captured under an AXIO microscope (AxioObserver A1, Carl Zeiss), which was equipped with Epi−fluorescence and AxioCam MRc imaging system. The fluorescence images were also taken by confocal laser scanning microscope (CLSM) and analyzed with OLYMPUS FLUOVIEW ver. 1.5 Viewer software.

MTT and lactase dehydrogenase (LDH) release assays were performed to evaluate the therapeutic efficiency of the complexes and to assess the cell membrane integrity, respectively. The details procedures on MTT and LDH release assays have been presented in ESI.

2.5. Characterization instruments

FTIR and UV−vis spectra were recorded on a Nexus 670 FT-IR spectrophotometer (Nicolet Instruments) using a KBr disk at a resolution of 4 cm^{-1} and a Cary 5000 UV−vis–NIR spectrophotometer (Varian), respectively. Fluorescence measurements were performed on a Cary Eclipse fluorescence spectrophotometer (Varian). The values of ζ potential were measured with a Zeta potential analyzer (Nano Z, Malvern).

3. Results and discussion

The goal of this work is to construct a GO-based anticancer drug loading and cell-specific delivery system using aptamer as a targeting agent. Before loading the drug, aptamer (A1) was covalently conjugated with GO based on EDC/NHS coupling. The conjugation of A1 on GO was confirmed by FTIR spectroscopy (Fig. 1A). FTIR spectrum of GO exhibits the characteristic vibrations of GO (curve a, Fig. 1A), including the stretching mode of O−H (~3410 cm^{-1}), stretching vibration of C=O at carboxylic group (~1725 cm^{-1}), sp^2 hybridized C=C (~1624 cm^{-1}), C–OH groups (~1223 cm^{-1}), and the deformation mode of C–O groups in epoxide moieties (~1054 cm^{-1}).[7–9,36] After conjugated with A1, we observe the characteristic peak of the amide bond:[7] the stretching vibration bands of C=O (~1640 cm^{-1}) and C–N (1382 cm^{-1}) for amide (curve b, Fig. 1A). We also observe the bands of the $–CH_2–$ spacer in A1 at ~2977 and 2930 cm^{-1}. However, the stretching vibration bands of C=O at carboxylic group (should be at ~1725 cm^{-1}) and epoxide moieties (should be at ~1054 cm^{-1}) of GO are absent from IR spectrum of A1−GO. These results demonstrate the chemical conjugation of A1 with GO. Moreover, the band of C=C vibration of aromatic rings is observed at ~1624 cm^{-1} in both GO and A1−GO spectra, implying the preservation of the sp^2 character in A1−GO after the chemical conjugation.

After conjugation with A1, we loaded DAC onto A1–GO by stirring the mixture of DAC and A1–GO. The loading process was characterized by UV–vis (Fig. 1B) and fluorescence spectra (Fig. 1C). Free GO, DAC, and A1 show the characteristic absorption peak at ~230 (curve a, Fig. 1B), 240 (curve b, Fig. 1B), and 260 nm (curve c, Fig. 1B), respectively, which are in good agreement with those reported previously.[9,39] After reacted with A1, FTIR spectrum shows an absorption peak at ~255 nm (curve d, Fig. 1B), do not show the characteristic absorption peak associated with GO, suggesting the conjugation of A1 with GO. After the loading of DAC, A1–GO/DAC complex exhibits an absorption peak at ~248 nm (curve e, Fig. 1B), locating between the characteristic peaks of free DAC and A1. In comparison with free DAC, the absorption peaks of DAC in A1–GO/DAC complex has ~8 nm red-shifts, which are generally believed due to the ground-state electron donor-acceptor interaction between the two components,[50] namely GO and DAC in this work. This interaction was also verified by fluorescence spectroscopy (Fig. 1C). Free DAC exhibits a fluorescence emission maximum at ~370 nm with an

excited source at 282 nm (curve a, Fig. 1C). However, A1–GO/DAC exhibits significant quenching of emission band (curve b, Fig. 1C), implying the presence of a photoinduced electron-transfer process or efficient energy transferring along the GO/DAC interface due to strong π–π stacking interaction between the two components.[51,52] These results indicate the loading of DAC onto A1–GO.

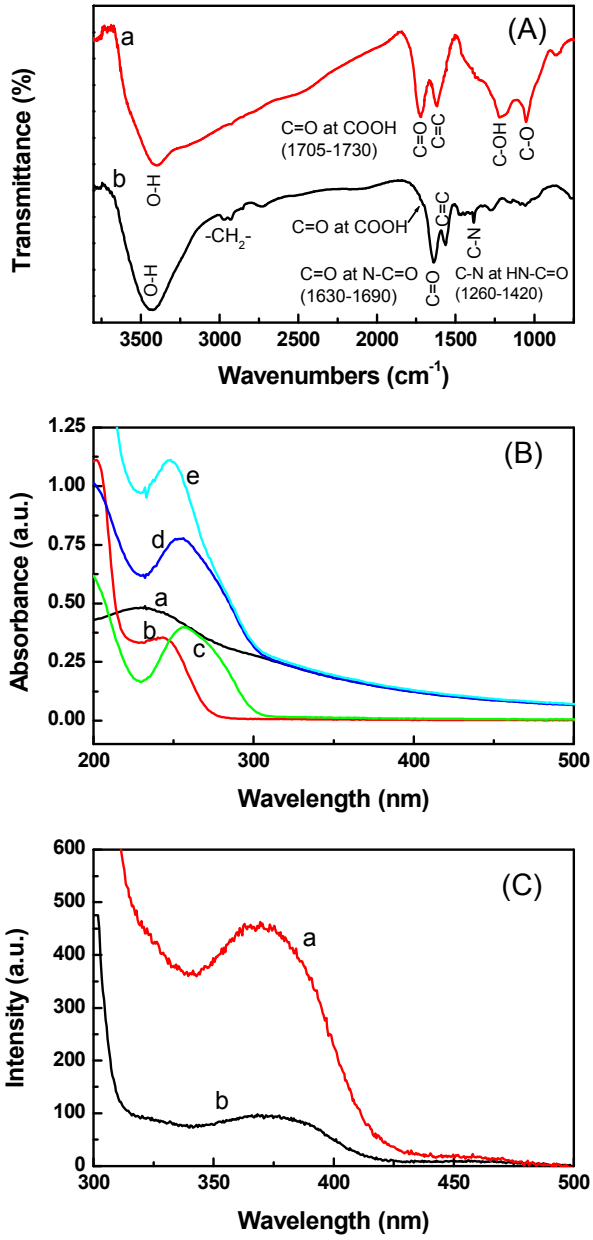

Fig. 1 (A) FTIR spectra of GO (a) and A1–GO (b). (B) UV–vis spectra of GO (a), free DAC (b), free A1 (c), A1–GO (d), and A1–GO/DAC complexes (e). (C) Fluorescence spectra of free DAC (a) and A1–GO/DAC complex (b) in water at an excitation wavelength of 282 nm. The concentrations of both A1–GO/DAC and DAC were controlled to be the same according to the loading capacity of DAC.

We also measured the ζ potential (at pH 7.4) to verified the conjugation of A1 with GO and the loading of DAC onto A1–GO. The ζ value of GO is ~–(37.1 ± 5.4) mV, this value increases to be ~(6.0 ± 2.1) mV after conjugation with A1. After loading of the DAC, the ζ value of A1–GO/DAC is ~(2.7 ± 1.9) mV (note that we measured the ζ value of the A1 and DAC alone is ~–(55.4 ± 5.6) and –(15.6 ± 3.9) mV, respectively. The ζ value of the mixture of GO and A1 (without presence of EDC and NHS) is ~–(44.6 ± 6.2) mV). These changes of ζ value provide additional evidence of the conjugation of A1 with GO and the loading of DAC onto the A1–GO surface.

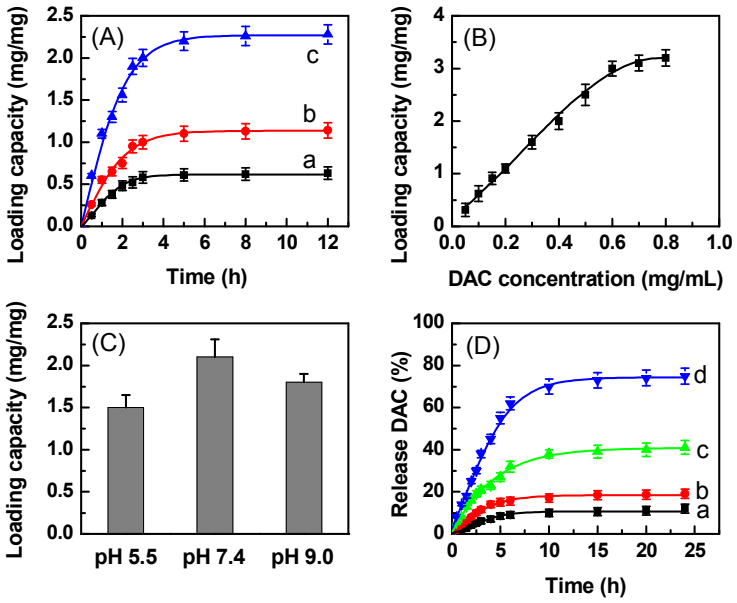

Fig. 2 (A) The loading kinetics of DAC onto A1–GO at DAC initial concentration of 0.1 (a), 0.2, and 0.4 mg/mL (c) in PBS (pH 7.4). The concentration of A1–GO was kept at 0.15 mg/mL. (B) Dependence of the loading capacity on DAC initial concentration. The data were obtained in PBS with pH 7.4. (C) Dependence of the loading capacity on solution pH. DAC initial concentration was 0.4 mg/mL. (D) Release kinetics of DAC from A1–GO/DAC complexes in PBS at pH value of 7.4 (a), 9.0 (c), and 5.5 (d). Curve (b) shows the release profile of DAC in 10% FBS/DMEM. Error bars were based on three measurements. Note that A1–GO/DAC used for release measurements was prepared by stirring the mixture of DAC solution (0.05 mg/mL, in PBS, pH 7.4) and A1–GO dispersed solution (0.15 mg/mL) for 12 h.

The loading kinetics was studied at three different initial DAC concentrations (0.1, 0.2, and 0.4 mg/mL) with keeping A1–GO concentration at 0.15 mg/mL. As shown in Fig. 2A, the loading features

are similar at DAC initial concentration of 0.1 (curve a, Fig. 2A), 0.2 (curve b, Fig. 2B), and 0.4 mg/mL (curve c, Fig. 2A). The loading of DAC takes place rapidly in the first 3 h and follows by a slower loading rate to reach a plateau at ~5 h. The loading capacity is ~0.6, 1.1, and 2.1 mg/mg at DAC initial concentration of 0.1, 0.2, and 0.4 mg/mL, respectively, corresponding to the loading efficiency of ~90, 83, and 79%, respectively (the loading efficiency is calculated using: loading efficiency = the mass of the loaded DAC / the total DAC mass used for loading × 100%). The saturated loading capacity is estimated to be ~3.0 mg/mg (corresponding to the loading efficiency of ~64%), which is attained at DAC initial concentration higher than 0.7 mg/mL (Fig. 2B). Although some surface areas on GO have obviously been occupied by A1 molecules, the loading capacity is still higher than that of some common drug carrier materials, such as liposomes, polymer vesicles, carbon nanohorns, where the loading capacity is always below 1 mg/mg at saturated carrying concentration.[9,10]

The high loading capacity of DAC onto A1–GO may be due to the strong π–π stacking interaction formed between the large π-conjugated structure of GO and DAC (the π–π interaction can be evidenced by the fluorescence quenching of DAC after loaded on A1–GO, Fig. 1C). In addition, the strong hydrogen-bonding interaction of –OH and –COOH groups on GO sheet with –OH and $–NH_2$ groups in DAC may also facilitate the loading of DAC and therefore enhance the loading capacity of the drug. Furthermore, the two faces and edges payload originated from the unique structure of GO also contributes to the enhancement of the loading capacity of the drug.

We also studied pH-dependent loading capacity of DAC. The measurement was conducted at DAC initial concentration of 0.4 mg/mL (A1–GO concentration was kept at 0.15 mg/mL) at pH 5.5, 7.4, and 9.0. As expected, A1–GO shows distinctly different loading capacity toward DAC at different pH values (Fig. 2C). The loading capacity is ~1.6, 2.1, and 1.8 mg/mg at pH 5.5, 7.4, and 9.0, respectively. The highest loading capacity is obtained at the neutral condition, rather than acidic or basic conditions. The pH-dependent loading capacity may be due to the different degree of hydrogen-bonding interaction between these two species under different pH conditions similar to the case of doxorubicin on GO[9] (please refer to ESI for the detailed analysis on hydrogen bonds formed between GO and DAC at

different pH). The results of Fig. 2C also indicate that the loading capacity is larger under basic conditions than that under acidic conditions, implying that hydrogen-bonding interaction under basic conditions is stronger than that under acid conditions.

The release kinetics of DAC from A1–GO/DAC complex was investigated in PBS under physiological (pH 7.4), acidic (pH 5.5. Note that pH of tumor site, usually 5.0−6.0, is lower than that of normal tissues because of the acidic lysosomes inside tumor cells[53]), and basic condition (pH 9.0. The reason of choosing pH 9.0 is that we intend to compare release features of DAC from A1–GO/DAC in basic condition with those in acidic and physiological conditions), and in cell culture medium (10% FBS/DMEM) (Fig. 2D). It can be seen that the release of DAC is a pH-dependent manner. The release rate is much slower at physiological condition (pH 7.4, curve a, Fig. 2D) than that at acidic (pH 5.5, curve d, Fig. 2D) and basic conditions (pH 9.0, curve c, Fig. 2D). Only ~10% of the total loaded DAC is released in 24 h under physiological condition (pH 7.4), implying the stability of DAC on A1–GO in physiological condition, and suggesting that it can be protected in the blood stream before reaching the targeted tumor site. The release efficiency of DAC in culture medium with 10% FBS is slightly higher (~18%, curve b, Fig. 2D) than that in PBS (at pH 7.4, curve a, Fig. 2D). This is likely due to the preferential binding of DAC molecules with serum proteins.[8] Since the cell interior contains even more organic compounds such as proteins, lipids and complex sugars, it is expected that the release of DAC from A1–GO/DAC complexes is even faster after cellular uptake to achieve a sufficient intracellular delivery. The release efficiency under basic (pH 9.0, curve c, Fig. 2D) and acidic solution (pH 5.5, curve d, Fig. 2D) is ~40% and 75%, respectively. As presented in ESI, the hydrogen-bonding interaction between DAC and GO is the strongest at the neutral condition, resulting in an inefficient release. The stronger hydrogen-bonding interaction under basic conditions than that under acidic conditions results in a low release efficiency in basic condition.

In addition, the surface charges of the A1–GO (ζ potential) may also have significant effects on its loading and release features for DAC. The values of ζ potential of A1–GO are ~(10.5 ± 3.2), (6.0 ± 2.1), and (3.6 ± 1.7) mV at pH 5.5, 7.4, and 9.0, respectively, indicating the ζ potential of A1–GO has a slight

negative shift with increasing of the solution pH (note that the values ζ potential of GO are ~–(23.3 ± 2.9), –(37.1 ± 5.4), and –(42.5 ± 4.6) mV at pH 5.5, 7.4, and 9.0, respectively). The values of ζ potential of DAC itself are ~–(5.1 ± 2.1), –(15.6 ± 3.9), and –(14.7 ± 3.5) mV at pH 5.5, 7.4, and 9.0, respectively. These changes of the ζ potential suggest that the solution pH can alter the surface charges of A1–GO and DAC, which can affect the interaction between the A1–GO and DAC, further determining the loading and release features of DAC.

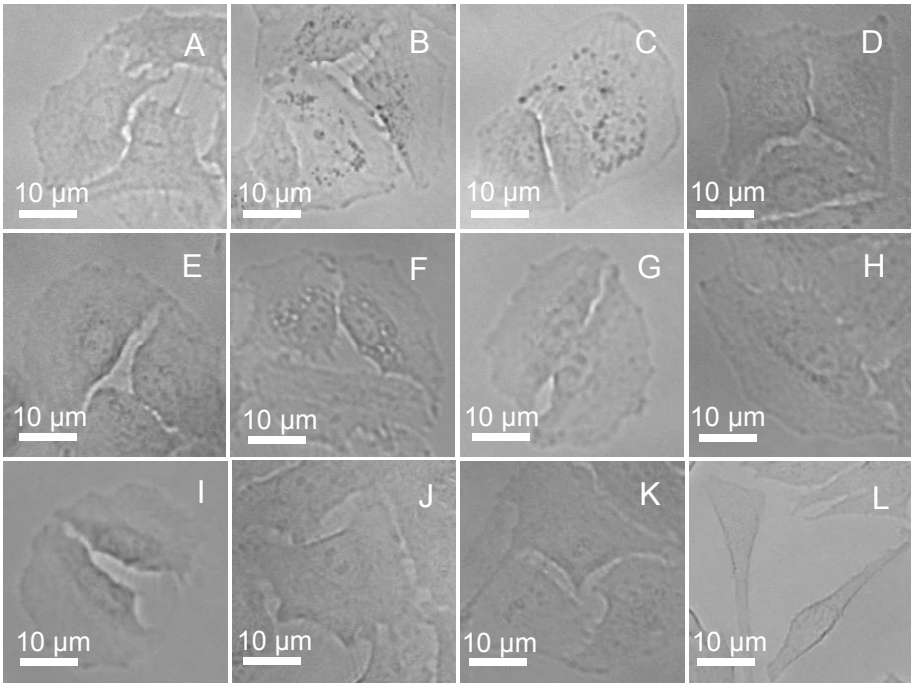

Fig. 3 BF images A549 cells before (A) and after incubation with 20 μg/mL A1–GO/DAC (B) for 2 h. (C)–(F) show BF images of A549 cells after 2 h incubation with 20 μg/mL A1–GO (C), free GO (D), GO/DAC (E), and free DAC (F), respectively. (G)–(L) show BF images of NCI-H157 (G), NCI-H520 (H), NCI-H1299 (I), NCI-H446 (J), MCF-7 (K), and HeLa cells (L), respectively, after 2 h incubation with A1–GO/DAC (20 μg/mL).

The pH-dependent DAC release feature renders the A1–GO/DAC complex a potential application for tumor therapy, since the pH of tumor site (pH = 5.0−6.0) is lower than that of normal tissues due to the acidic lysosomes inside tumor cells.[53] The complexes first specifically transport to the cancer cells, and then bind with the cancer cells. At lysosomal acidic pH (5.0–6.0), protonation of amine groups on DAC breaks the part of the hydrogen bond between DAC and GO carrier, leading to a desired release of the

drug. In view of the different releasing behaviors of DAC under different environments, the complexes can be used as a good candidate material for intelligent drug release.

The targeting of the A1–GO/DAC complexes to specific cancer cells was demonstrated by selective binding of the complexes to A549 cells, which was first evidenced by the morphological changes of the cells. Bright-field (BF) microscopic images show that the surface of the cells is clear before they were incubated with the complexes (Fig. 3A. Note that BF images at a low magnification are presented in Fig. S3, ESI), while the surface of the cells are observed to be decorated with many small dark dots after incubated with the complexes (Fig. 3B). These dark dots are the aggregates of the complexes on cell surface because many A1–GO/DAC complexes could to be bound to one cell. These results indicate the binding of the complexes onto the cell surface. This binding process is further verified by TEM images, which show several dark nanoclusters on cell surface after the cells were incubated with the complexes (Fig. S4A, ESI), while the cell surface is clear before incubation (Fig. S4B, ESI).

To demonstrate the binding of the complexes onto the cell surface is due to the specific interaction of A1 with A549 cells, we incubated the cells with A1–GO, free GO, GO/DAC, and free DAC, respectively, for 2 h. After washed with PBS, BF images were recorded (Fig. 3C–F). The results show that there are also some dark dots on cell surface after incubated with A1–GO (Fig. 3C), implying aggregation of A1–GO on cell surface due to the specific interaction between A1 and the cells. In contrast, the surface of the cells is clear after they were incubated with GO (Fig. 3D), GO/DAC (Fig. 3E), and free DAC (Fig. 3F), suggesting that no aggregate is formed on cell surface due to the lack of the specific interaction of A1 in these cases, demonstrating the specific interaction of A1 with A549 cell causes the binding of the A1–GO/DAC complexes on the cell surface.

We also employed the confocal laser scanning microscope (CLSM) technique to verify the binding of the A1–GO/DAC complexes to A549 cells because the GO emits the blue fluorescence under an excitation of 405 nm. A549 cell itself emits the weak blue fluorescence under an excitation at 405 nm (Fig. 4A), probably due to some proteins at cell membrane emitting the fluorescence under this excitation. After the cell incubated with GO, we can observe a very slightly increased blue fluorescence

(Fig. 4B). However, the blue fluorescence intensity has an obvious enhancement after the cell incubated with A1–GO (Fig. 4C), or A1–GO/DAC (Fig. 4D), indicating that the A1–GO and A1–GO/DAC have an strong interaction with the cell due to the presence of A1, which has specific interaction with the cell. Moreover, CLSM images in Fig. 4B–D also indicate that GO, A1–GO, or A1–GO/DAC does not enter into the inside of A549 cell, otherwise, we can observe the blue fluorescence inside the cell. The reason that the GO does not enter into the inside of the cell is probably due to the relative large GO sheets (20 nm) we used.

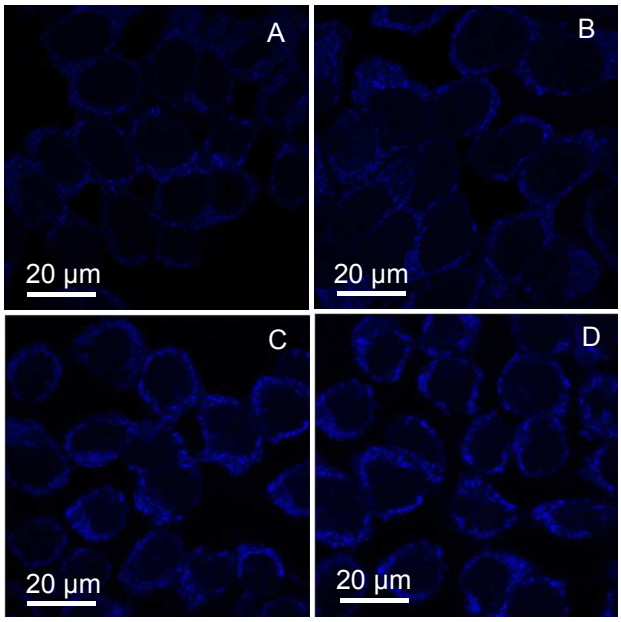

Fig. 4 CLSM images A549 cells before (A) and after incubation with 20 μg/mL GO (B), A1–GO (C), and A1–GO/DAC (D), respectively, for 2 h. Before recording the images, the cells were washed thrice with PBS. The images were captured under an excitation at 405 nm.

The specific interaction of A1 with A549 cells was further demonstrated by fluorescence images. We labeled the A1–GO/DAC complexes with Rhodamine 6G (Rh6G) by mixing 10 μL of Rh6G solution (10 μM) with 2 mL of A1–GO/DAC suspension (0.5 mg/mL) and stirring for 30 min. After the Rh6G-labeled complexes were collected by centrifugation and incubated with A549 cells for 2 h, the fluorescence images were captured with an excitation at 543 nm. A549 cell itself shows no fluorescence emission (Fig. S5A, ESI), however, we observe red fluorescence emitted from Rh6G after the cells were incubated with Rh6G-labeled complexes (Fig. S5B, ESI), indicating that the Rh6G-labeled complexes

have bound onto the surface of the cells due to the specific interaction of A1 with the cells. As control, we also labeled the A1–GO and GO with Rh6G, and incubated them with A549 cells. The fluorescence images show that a red fluorescence emission can also be observed after the cells were incubated with Rh6G-labeld A1–GO (Fig. S5C, ESI), while almost no fluorescence emission can be seen in the case of GO due to the lack of the specific interaction of A1 with the cells. These results verify that the binding of the A1–GO/DAC complexes is due to the specific interaction of A1 with A549 cells, which is consistent with that obtained from BF and TEM images.

We also conjugated GO with a synthesized oligonucleotides A2 (having one-base mismatch in comparison with A1), A3 (having three-base mismatch in comparison with A1), and sgc8 and tdo5 aptamer (the detailed sequences are depicted in Table 1), respectively, and then loaded DAC. After incubated with A549 cells for 2 h, BF and CLSM images were recorded. BF images depicted in Fig. S6A–D (ESI) show that the morphologies of the cells remain almost unchanged compared with those before incubation (as depicted in Fig. 3A), indicating that these complexes cannot bind to A549 cells because of the lack of the specific aptamer of the cell. CLSM images depicted in Fig. S6E–H (ESI) also indicate that the blue fluorescence intensity of the cells is very weak after the cells were incubated with 20 μg/mL A2–GO/DAC (Fig. S6E, ESI), A3–GO/DAC (Fig. S6F, ESI), sgc8–GO/DAC (Fig. S6G, ESI), or tdo5–GO/DAC (Fig. S6H, ESI) for 2 h. The fluorescence intensity does not show any enhancement in comparison with that of the A549 cell itself (Fig. 4A), also due to that these complexes cannot bind to A549 cells because of the lack of the specific aptamer of the cell.

To further verify that the A2–GO/DAC, A3–GO/DAC, sgc8–GO/DAC, and tdo5–GO/DAC complexes cannot not be effectively bound with A549 cells, we labeled these complexes with Rh6G by mixing 10 μL of Rh6G solution (10 μM) with 2 mL of A1–GO/DAC suspension (0.5 mg/mL) and stirring for 30 min. After the cells were incubated with these Rh6G-labeled complexes for 2 h, the fluorescence images were recorded (under an excitation of 543 nm). The results presented in Fig. S6I–L (ESI) show that almost no fluorescence emission can be observed, further verifying that these complexes cannot be bound to the cell surface.

The binding of the A1–GO/DAC complexes on the surface of the A549 cells is high specific. We incubated the complexes with NCI-H157 (squamous carcinoma cell, NSCLC), NCI-H520 (squamous carcinoma cell, NSCLC), NCI-H1299 (large cell carcinoma cell, NSCLC), NCI-H446 (SCLC), MCF-7 (human breast carcinoma cell), and HeLa (human cervical carcinoma cell), respectively. BF images show that the complexes cannot bind on the surface of these cells because no any aggregates of the complexes can be found on the surface of these cells (Fig. 3G–L). These results suggest that the A1–GO/DAC complexes have the ability to recognize A549 cells from other types of cancer cells (HeLa and MCF-7 cells) and subtypes of lung cancer cells (NCI-H157, NCI-H520, NCI-H1299, and NCI-H446 cells). The recognition and identification of the biological heterogeneity of lung cancer subtypes will enable the complexes to be used for specific therapy of lung cancer.

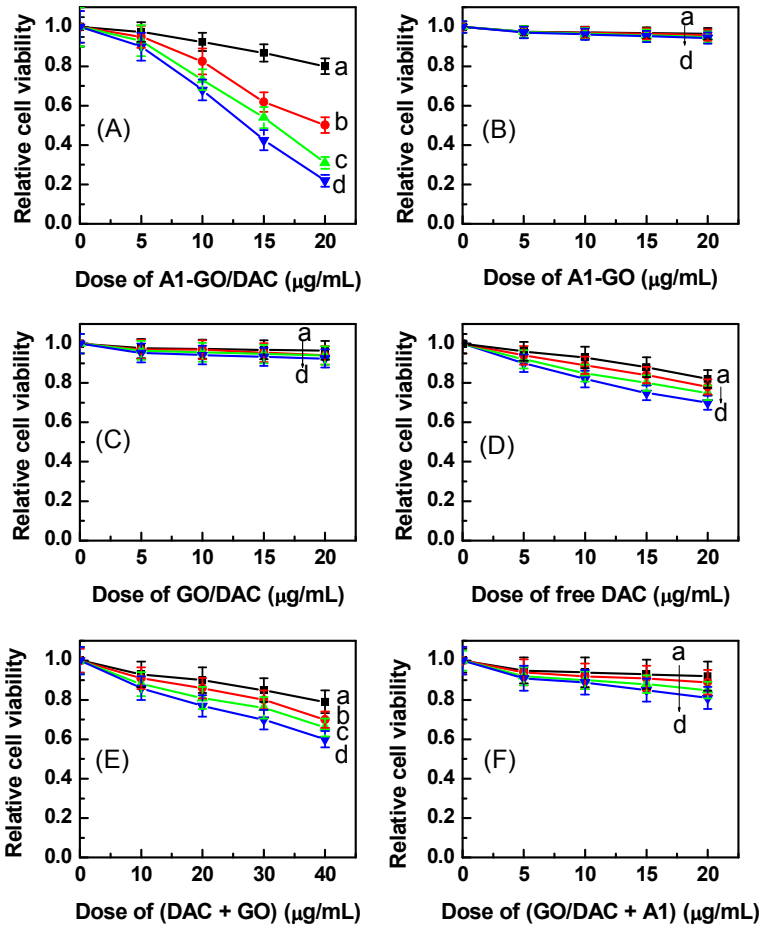

Fig. 5 Dose-dependent cell viability of A549 cells incubated with A1–GO/DAC complexes (A), A1–GO (B), GO/DAC (C), free DAC (D), and the mixture of free DAC and GO (at equal dose of DAC and GO)

(E), and the mixture of GO/DAC and A1 (F, the concentration of A1 is 1 μM). The incubation time is 4 (curve a), 8 (curve b), 16 (curve c), and 24 h (curve d). Error bars were based on three measurements.

We then investigated the antitumor activity of the A1–GO/DAC complexes by MTT assay. The results presented in Fig. 5 demonstrate that the toxicity of the complexes to A549 cells displays dose- and incubation time-dependent manners (Fig. 5A). The cell viability decreases with the increase of the incubation time and the dose of the complexes in the cell culture medium. The viability is ~80, 50, 31, and 22% (at the complex dose of a 20 μg/mL) at the incubation time of 4, 8, 16, and 24 h, respectively. For comparison, we also examined cytotoxicity of A1–GO, GO/DAC, and free DAC to A549 cell. It is indicated that the toxicity of A1–GO is negligible even at the highest dose of our experiments (20 μg/mL) and the longest incubation time of 24 h (Fig. 5B). This result is in agreement with those previous reports, which showed that GO has no obvious cytotoxicity at a concentration of lower than an 80 μg/mL.[36–38] The toxicity of GO/DAC and free DAC is significantly lower than that of the A1–GO/DAC complexes because the cell viability still remains ~93 (for GO/DAC, Fig. 5C) and 75% (for free DAC, Fig. 5D), respectively, after 24 h incubation (at dose of 20 μg/mL). These results suggest that the antitumor activity of A1–GO/DAC complexes is greatly improved in comparison with GO/DAC and free DAC due to the specific binding of A1 to the target cell and effective release of the drug.

We also evaluated the antitumor activity of the mixture of free DAC and GO (at equal dose of the DAC and GO), and the mixture of GO/DAC and A1 (the concentration of A1 was 1 μM) to A549 cells by incubating the cells in the mixture for a certain time, and then the MTT measurements were carried out. The results indicated that the cytotoxicity of the mixture of DAC + GO (Fig. 5E) and mixture of GO/DAC + A1 (Fig. 5F) was much lower than that of A1–GO/DAC complexes (Fig. 5A) because the cell viability still remains more than 60 (for the mixture of DAC and GO, Fig. 5E) and 80% (for mixture of GO/DAC + A1, Fig. 5F), respectively, even after 24 h incubation (at dose of 20 μg/mL). These results further demonstrate the important role of the specific binding of A1 to the target cell for antitumor activity of A1–GO/DAC complexes.

We further evaluated the antitumor activity of the A2–GO/DAC, A3–GO/DAC, sgc8–GO/DAC, and tdo5–GO/DAC complexes to A549 cells by incubating the cells with these complexes (at 20 μg/mL) for certain time (0–24 h). MTT results indicate that the toxicity of these complexes is very low and almost negligible because the cell viability still remains ~85 (for A2–GO/DAC, curve a in Fig. S7, ESI), ~92 (for A3–GO/DAC, curve b in Fig. S7, ESI), ~96 (for sgc8–GO/DAC, curve c in Fig. S7, ESI), and ~96 % (for tdo5–GO/DAC, curve d in Fig. S7, ESI), respectively, even after 24 h incubation at a dose of 20 μg/mL, implying that these complexes cannot bind to A549 cells because of the lack of the specific aptamer of the cell. This result is in good agreement with those obtained from BF, CLSM, and fluorescence images depicted in Fig. S6 (ESI).

The antitumor activity of the A1–GO/DAC complexes can be further evidenced by the cell morphology observations. Differential interference contrast (DIC) images show the damage of the cell membrane (Fig. 6A–F) after the cell was incubated with the A1–GO/DAC complexes (at a dose of 20 μg/mL). This cell membrane damage, which is observed clearly from high-magnification DIC image (Fig. 6F), is caused by the complex-induced cell death. Moreover, the degree of membrane damage increases with the increasing of the incubation time (Fig. 6B–E), indicative of the increased cell mortality following the incubation time. After 24 h incubation, most of the cells are dead (Fig. 6E). In contrast, we observed no destruction for those cells incubated with 20 μg/mL A1–GO (Fig. 6G) or GO/DAC (Fig. 6H) for 24 h. The fraction of the dead cell is low after the cells were incubated with free DAC (20 μg/mL) (Fig. 6I), DAC + GO (each at 20 μg/mL) (Fig. 6J), or GO/DAC (20 μg/mL) + A1 (1 μM) (Fig. 6K) for 24 h. These results suggest that the antitumor activity of the A1–GO/DAC complexes is significant high in comparison with that of A1–GO, GO/DAC, free DAC, the mixture of DAC and GO, or GO/DAC and A1, which is in good agreement with that concluded from the MTT assay.

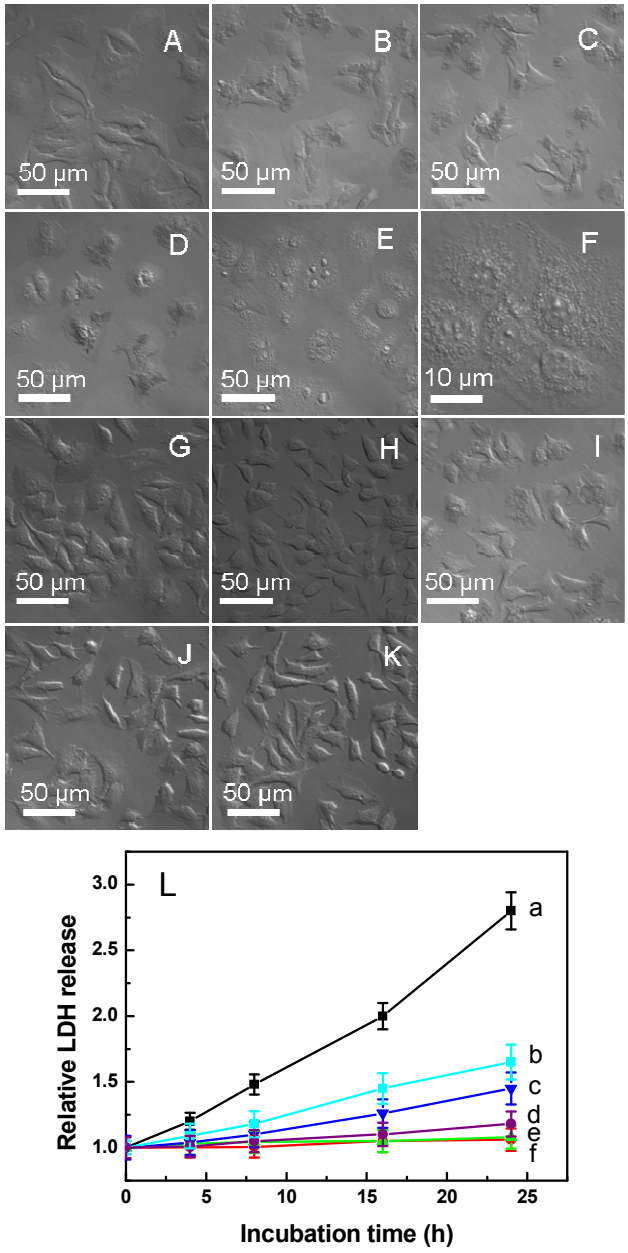

Fig. 6 DIC images of A549 cells incubated with 20 μg/mL of A1–GO/DAC complexes for 0 (A), 4, (B), 8 (C), 16 (D), and 24 h (E). (F) DIC image of A549 cell after incubated with the complexes for 24 h under a high magnification. (G)–(K) show DIC images of the cells after incubated with A1–GO (G), GO/DAC (H), free DAC (I), the mixture of free DAC and GO (at equal dose of DAC and GO) (J), and the mixture of GO/DAC and A1 the concentration of A1 is 1 μM) (K), respectively, for 24 h (each at dose of 20 μg/mL). (L) Incubation time-dependent LDH release for A549 cells incubated with A1–GO/DAC complexes (a), free DAC + GO (b, each at 20 μg/mL), free DAC (c), GO/DAC + A1 (1 μM) (d), GO/DAC (e), and A1–GO (f) at dose of a 20 μg/mL. LDH release was expressed relative to the basal LDH release from untreated cells. Error bars were based on three measurements.

To demonstrate cell death presented in Fig. 6 is due to the A1–GO/DAC-induced membrane damage (necrosis), we recorded the morphological changes of the cell natural death process (Fig. S8, ESI). In the process of cell natural death, the cell produces many neurites (Fig. S8A, B, and C, ESI), and then undergoes shrinkage and the neurite length increases (Fig. S8D, E, ESI), finally the cell becomes round in shape (Fig. S8F, ESI), indicating death of the cell. However, the cell membrane of the dead cells remains integrated (Fig. S8F, ESI), which is different from that A1–GO/DAC-induced cell death. To further confirm that the A1–GO/DAC complexes inducing cell membrane damage, we performed LDH release measurement, which is a cell membrane damage marker.[5,30,31] LDH release is significant following the treatment of the A1–GO/DAC complexes, and increases with the increasing of the incubation time (curve a, Fig. 6L). However, the LDH release is at a low when the cells were treated with free DAC + GO (each at 20 μg/mL, curve b, Fig. 6L) or free DAC (at 20 μg/mL, curve c, Fig. 6L). It is at a negligible level when the cells were incubated with GO/DAC (20 μg/mL) + A1 (1 μM) (curve d, Fig. 6L), GO/DAC (at 20 μg/mL, curve e, Fig. 6L), and A1–GO (at 20 μg/mL, curve f, Fig. 6L). These results indicate the high degree of the membrane damage induced by A1–GO/DAC complexes, verifying high efficacy of the complexes for chemotherapy of the specific cancer.

4. Conclusions

In summary, we have developed an anticancer drug loading and cell-specific delivery systems based on cell-type-specific aptamer-functionalized GO. The loading capacity of DAC on GO surface is pH- and DAC initial concentration-dependent with the saturated loading capacity attained under physiological condition (pH 7.4). The release of DAC from the complexes is also pH-dependent with a quicker rate at acidic pH condition (pH 5.5) than at physiological pH condition. The complexes can specifically recognize A549 cells from other types of cancer cells and subtypes of lung cancer cells due to the specific binding of the aptamer with the cells. Importantly, the formed complexes exhibit a much higher therapeutic efficacy in inhibiting the growth of the cancer cells by inducing the cell membrane damage than free DAC drug. The high DAC payload and antitumor efficacy render our developed system promising for different biomedical applications. Moreover, with aptamer being available for any kind of

target, the developed approach here may become a general route for delivery of various anticancer drugs for a range of cancer therapy.

Acknowledgements

This work is supported by NSFC (21175067, 21273117, 21335004, and 21375063), the Research Fund for the Doctoral Program of Higher Education of China (20103207110004), NSF of Jiangsu Province (BK2011779), China Postdoctoral Science Foundation (2013M541695), the Foundation of the Jiangsu Education Committee (13KJB150024), the Program for Outstanding Innovation Research Team of Universities in Jiangsu Province, and the Priority Academic Program Development of Jiangsu Higher Education Institutions.

References

1 J. Ferlay, H. R. Shin, F. Bray, D. Forman, C. Mathers and D. M. Parkin, *Int. J. Cancer*, 2010, **127**, 2893-2917.

2 J. Zhang, Z.-F. Yuan, Y. Wang, W.-H. Chen, G.-F. Luo, S.-X. Cheng, R.-X. Zhuo and X.-Z. Zhang, *J. Am. Chem. Soc.*, 2013, **135**, 5068-5073.

3 B. Kang, M. M. Afifi, L. A. Austin and M. A. El-Sayed, *ACS Nano*, 2013, **7**, 7420-7427.

4 E. C. Dreaden, A. M. Alkilany, X. H. Huang, C. J. Murphy and M. A. El-Sayed, *Chem. Soc. Rev.*, 2012, **41**, 2740-2779.

5 M. Nurunnabi, Z. Khatun, K. M. Huh, S. Y. Park, D. Y. Lee, K. J. Cho and Y.-K. Lee, *ACS Nano*, 2013, **7**, 6858-6867.

6 J.-J. Zhang, T.-T. Zheng, F.-F. Cheng, J.-R. Zhang and J.-J. Zhu, *Anal. Chem.*, 2011, **83**, 7902-7909.

7 H. Kim, D. Lee, J. Kim, T. Kim and W. J. Kim, *ACS Nano*, 2013, **7**, 6735-6746.

8 X. T. Zhang and C. M. Li, *Mol. Pharmaceutics*, 2012, **9**, 615-621.

9 X. Yang, X. Zhang, Z. Liu, Y. Ma, Y. Huang and Y. Chen, *J. Phys. Chem. C*, 2008, **112**, 17554-17558.

10 X. Yang, Y. Wang, X. Huang, Y. Ma, Y. Huang, R. Yang, H. Duan and Y. Chen, *J. Mater. Chem.*, 2011, **21**, 3448-3454.

11 Z. Liu, J. T. Robinson, X. Sun and H. Dai, *J. Am. Chem. Soc.*, 2008, **130**, 10876-10877.

12 J. Chen, S. Chen, X. Zhao, L. V. Kuznetsova, S. S. Wong and I. Ojima, *J. Am. Chem. Soc.*, 2008, **130**, 16778-16785.

13 L. Yuan, W. Chen, J. Hu, J. Z. Zhang and D. Yang, *Langmuir*, 2013, **29**, 734-743.

14 Y. Wang, K. Wang, J. Zhao, X. Liu, J. Bu, X. Yan and R. Huang, *J. Am. Chem. Soc.*, 2013, **135**, 4799-4804.

15 W. Liu, X. Li, Y.-S. Wong, W. Zheng, Y. Zhang, W. Cao and T. Chen, *ACS Nano*, 2012, **6**, 6578-6591.

16 Z. Li, Z. Liu, M. Yin, X. Yang, Q. Yuan, J. Ren and X. Qu, *Biomacromolecules*, 2012, **13**, 4257-4263.

17 S. Wang, Y. Wu, R. Guo, Y. Huang, S. Wen, M. Shen, J. Wang and X. Shi, *Langmuir*, 2013, **29**, 5030-5036.

18 H. Kim, R. Namgung, K. Singha, I.-K. Oh and W. J. Kim, *Bioconjugate Chem.*, 2011, **22**, 2558-2567.

19 C. Wang, H. Xu, C. Liang, Y. Liu, Z. Li, G. Yang, L. Cheng, Y. Li and Z. Liu, *ACS Nano*, 2013, **7**, 6782-6795.

20 Z. Cao, R. Tong, A. Mishra, W. Xu, G. C. L. Wong, J. Cheng and Y. Lu, *Angew. Chem. Int. Ed.*, 2009, **48**, 6494 -6498.

21 N. Nasongka, X. Shuai, H. Ai, B. D. Weinberg, J. Pink, D. A. Boothman and J. Gao, *Angew. Chem.*, 2004, **116**, 6483-6487.

22 T. R. Daniels, T. Delgado, G. Helguera and M. L. Penichet, *Clin. Immunol.*, 2006, **121**, 159-176.

23 K. A. Janes, P. Calvo and M. J. Alonso, *Adv. Drug Delivery Rev.*, 2001, **47**, 83-97.

24 M. Licciardi, G. Giammona, J. Du, S. P. Armes, Y. Tang and A. L. Lewis, *Polymer*, 2006, **47**, 2946-2955

25 S. Maiti, N. Park, J. H. Han, H. M. Jeon, J. H. Lee, S. Bhuniya, C. Kang, J. S. Kim, *J. Am. Chem. Soc.*, 2013, **135**, 4567-4572.

26 P. Sapra and T. M. Allen, *Cancer Res.*, 2002, **62**, 7190-7194.

27 T. A. Elbayoumi and V. P. Torchilin, *Eur. J. Pharm. Sci.*, 2007, **32**, 159-168.

28 P. Sapra and T. M. Allen, *Prog. Lipid Res.*, 2003, **42**, 439-462.

29 D. B. Kirpotin, D. C. Drummond, Y. Shao, M. R. Shalaby, K. Hong, U. B. Nielsen, J. D. Marks, C. C. Benz and J. W. Park, *Cancer Res.*, 2006, **66**, 6732-6740.

30 P. Wu, Y. Gao, Y. Lu, H. Zhang and C. Cai, *Analyst*, 2013, **138**, 6501-6510.

31 P. Wu, Y. Gao, H. Zhang and C. Cai, *Anal. Chem.*, 2012, **84**, 7692-7699.

32 L. Peng, C. S. Wu, M. You, D. Han, Y. Chen, T. Fu, M. Ye and W. Tan, *Chem. Sci.*, 2013, **4**, 1928-1938.

33 A. B. Iliuk, L. Hu and W. A. Tao, *Anal. Chem.*, 2011, **83**, 4440-4452.

34 F. Gu, L. Zhang, B. A. Teply, N. Mann, A. Wang, A. F. Radovic-Moreno, R. Langer and O. C. Farokhzad, *Proc. Natl. Acad. Sci. U. S. A.*, 2008, **105**, 2586-2591.

35 J. Guo, X. Gao, L. Su, H. Xia, G. Gu, Z. Pang, X. Jiang, L. Yao, J. Chen and H. Chen, *Biomaterials*, 2011, **32**, 8010-8020.

36 H. Liu, P. Xi, G. Xie, Y. Shi, F. Hou, L. Huang, F. Chen, Z. Zeng, C. Shao and J. Wang, *J. Phys. Chem. C*, 2012, **116**, 3334-3341.

37 M. Lv, Y. Zhang, L. Liang, M. Wei, W. Hu, X. Li and W. Huang, *Nanoscale*, 2012, **4**, 3861-3866.

38 W. Hu, C. Peng, M. Lv, X. Li, Y. Zhang, N. Chen, C. Fan and Q. Huang, *ACS Nano*, 2011, **5**, 3693-3700.

39 D. K. Rogstad, J. L. Herring, J. A. Theruvathu, A. Burdzy, C. C. Perry, J. W. Neidigh and L. C. Sowers, *Chem. Res. Toxicol.*, 2009, **22**, 1194-1204.

40 H. Kantarjian, J.-P. J. Issa, C. S. Rosenfeld, J. M. Bennett, M. Albitar, J. Dipersio, V. Klimek, J. Slack, C. de Castro, F. Ravandi, R. Helmer, L. Shen, S. D. Nimer, R. Leavitt, A. Raza, H. Saba, *Cancer*, 2006, **106**, 1794-1803.

41 H. M. Kantarjian, S. O'Brien, J. Cortes, F. J. Giles, S. Faderl, J.-P. J. Issa, G. Garcia-Manero, M. B. Rios, J. Shan, M. Andreeff, M. Keating and M. Talpaz, *Cancer*, 2003, **98**, 522-528.

42 D. S. Schrump, M. R. Fischette, D. M. Nguyen, M. Zhao, L. Xinmin, T. F. Kunst, A. Hancox, J. A. Hong, C. A. Chen, V. Pishchik, W. D. Figg, A. J. Murgo and S. M. Steinberg, *Clin. Cancer Res.*, 2006, **12**, 5777-5785.

43 S. V. Sharma, D. V. Bell, J. Settleman and D. A. Haber, *Nat. Rev. Cancer*, 2007, **7**, 169-181.

44 A. C. Borczuk and C. A. Powell, *Proc. Am. Thorac. Soc.*, 2007, **4**, 127-132.

45 Z. Zhao, L. Xu, X. Shi, W. Tan, X. Fang and D. Shangguan, *Analyst*, 2009, **134**, 1808-1814.

46 Z. Tang, D. Shangguan, K. Wang, H. Shi, K. Sefah, P. Mallikratchy, H. W. Chen, Y. Li, W. Tan, *Anal. Chem.*, 2007, **79**, 4900-4907.

47 Y. Hu, P. Wu, Y. Yin, H. Zhang and C. Cai, *Appl. Catal. B: Environmental*, 2012, **111-112**, 208-217.

48 P. Wu, Z. Cai, Y. Gao, H. Zhang and C. Cai, *Chem. Commun.*, 2011, **47**, 11327-11329.

49 P. Wu, Y. Qian, P. Du, H. Zhang and C. Cai, *J. Mater. Chem.*, 2012, **22**, 6402-6412.

50 D. M. Guldi, M. Marcaccio, D. Paolucci, F. Paolucci, N. Tagmatarchis, D. Tasis, E. Vázquez and M. Prato, *Angew. Chem., Int. Ed.*, 2003, **42**, 4206-4209.

51 Y. Lu, X. Yang, Y. Ma, Y. Huang and Y. Chen, *Biotechnol. Lett.*, 2008, **30**, 1031-1035.

52 D. Baskaran, J. W. Mays, X. P. Zhang and M. S. Bratcher, *J. Am. Chem. Soc.*, 2005, **127**, 6916-6917.

53 F. H. Chen, L. M. Zhang, Q. T. Chen, Y. Zhang and Z. J. Zhang, *Chem. Commun.*, 2010, **46**, 8633-8635.